IEEE Access
Multidisciplinary ⋮ Rapid Review ⋮ Open Access Journal

Received 10 June 2024, accepted 26 June 2024, date of publication 2 July 2024, date of current version 17 September 2024.

Digital Object Identifier 10.1109/ACCESS.2024.3421937

RESEARCH ARTICLE

Sensorless Predictive Multiscalar-Based Control of the Five-Phase IPMSM

DEEPAK VYAS[1], MARCIN MORAWIEC[1], (Senior Member, IEEE), GRZEGORZ KOSTRO[1], ANDRZEJ JĄDERKO[2], AND JANUSZ BARAN[2]

[1]Gdansk University of Technology, 80-233 Gdańsk, Poland
[2]Czestochowa University of Technology, 42-201 Częstochowa, Poland

Corresponding author: Deepak Vyas (deevyas@pg.edu.pl)

ABSTRACT This article proposes multi-scalar variables based predictive control of sensorless multiphase interior permanent magnet synchronous machine. Estimated parameters from adaptive observers are used to implement the proposed control scheme. The control approach is divided into two parts: for the fundamental plane, torque and its dual quantity from the multi-scalar model are directly predicted by the controller, and torque density is improved by injecting a third harmonic current in the second plane. The multi-scalar model of the 3rd harmonic plane is controlled by classical linear controllers. The analysis of the five-phase interior permanent magnet synchronous machine is done deeply in the stationary reference frame. Moreover, the proposed control scheme is compared with traditional predictive control-based field-oriented control for the fundamental plane and the field-oriented control (linear controllers-based) for the second plane in the $(d-q)$ reference frame. Compared with the previous control strategy, the proposed control structure provides a fast-dynamic response, reduces the computation resources by eliminating the reference frame transformation to obtain control signals, and improves overall control dynamics. The performance of the proposed control scheme is formally validated by simulation and experimental results.

INDEX TERMS Five-phase interior permanent magnet synchronous machine, multi-scalar, predictive torque control, field-oriented control, third harmonic current injection, sensorless control.

I. INTRODUCTION

Multiphase machines have received remarkable appreciation from researchers worldwide due to various benefits such as higher torque density, high fault tolerance capability, reduction in DC link stress, less torque ripple, improved reliability, and power density. These notable advantages of multiphase machines can be very helpful in industrial applications, electric vehicles, marine propulsion, and aerospace [1], [2], [3]. One of the most well-known representatives in this field is a five-phase interior permanent magnet synchronous motor (IPMSM), which offers a high torque density, rapid dynamic response, high reliability, and good power factor.

In a multiphase machine, space vectors can depict each current harmonic component separately. Power density can be improved by injecting harmonic current in a multiphase permanent magnet synchronous motor drive (PMSM) [4]. The output torque can be increased by injection of harmonic current. The harmonic order lower than the number of phases is mainly used [5]. Third, harmonic current injection with fundamental current increases output torque up to 10% to 17% compared to a three-phase machine of similar size [6].

Model predictive control (MPC) works on the principles of the predictive model, receding horizon, and feedback correction [7]. MPC is an online optimization control algorithm. For IPMSM drives, MPC can be categorized into two parts: continuous control set MPC, and finite control set MPC. Among them, the finite control set MPC is an attractive option as it uses the discrete model of the system to predict the trajectories of controlled variables with a finite set of control actuation [8]. MPC is one of the popular control techniques due to its fast-dynamic response and simple implementation.

When control objectives are selected based on torque and flux, it is called predictive torque control (PTC) [9]. PTC differs from direct torque control (DTC) as DTC requires hysteresis controllers and a switching table, while in PTC, predictive controllers and cost function online optimization are used. Weighting factors are needed in PTC to adjust

The associate editor coordinating the review of this manuscript and approving it for publication was Feifei Bu.

the torque and flux control proportion. Incorrect weighting factors lead to poor control performance of the whole system. The proposed control scheme in this article does not require a weighting factor. Research has been carried out for three-phase electric drives using MPC [7]. This article uses MPC for five-phase IPMSM to predict torque and its opposite quantity based on the multi-scalar variables.

Most of the research on the multiphase machine is focused on improving fault-tolerant capability [10], [11], [12], [13]. The field-oriented control (FOC) strategy is a highly used control strategy in which the state variables are oriented in a rotating reference frame *(d-q)* [3]. Direct torque control (DTC) is a popular alternative technique adapted by industries for the control of multiphase machines [14], [15], [16]. For fast dynamic response and accurate tracking of linear nonlinear systems, a generalized deadbeat solution was proposed for the MPC of five-phase PMSM drive [17]. In [18], Luo et al. proposed the control technique for six-phase PMSM based on MPC with a Luenberger observer to compensate for the localization error of the reference vector caused by the machine parameter mismatch. This technique improved the steady-state performance and robustness significantly.

For six-phase PMSM, disturbance observer-based predictive current control was reported in [19] to reduce the steady-state errors and harmonics in current. With significant errors in system parameters and different values of dead time in the power converter, this control scheme provided reliable performance. Song et al. reported that the 28^{th} order of the flux density spatial harmonics components causes the most vibration. In [13], the noise and vibration prediction of six-phase IPMSM was carried out for healthy mode and controlled faulty mod.

This article proposes sensorless predictive torque control (PTC) using multi-scalar variables for the fundamental plane and linear controller-based multi-scalar control for the second plane of five-phase IPMSM drives. The proposed technique predicts the multi-scalar variables such as torque and its dual quantity. Due to similar dimensions of predicted quantities, weighting factors are not required. In addition, classical predictive current control-based field-oriented control for the first plane and field-oriented control using PI controllers for the second plane is also implemented and compared with the proposed control scheme. The adaptive virtual observer for both planes is used to reconstruct stator currents, angular speeds, and angular positions. Estimated parameters minimize the disadvantages of measurement noise, gain drift, and reliability issues caused by sensors. The proposed control solution has certain limitations: 1) parameter mismatch may lead to error in predicting the value of torque and introduce ripple in torque. 2) implementation of the proposed control scheme is not straightforward in engineering practice due to the extensive sensorless control structure. The proposed concept is verified through analytical and simulation results and validated by experimentation on a five-phase IPMSM 5.5 kW machine.

The main contributions of the paper are:

1) Proposition of a new predictive multiscalar-based control strategy for five-phase IPMSM
2) Elimination of weighting factor in the proposed control scheme to achieve a good dynamic response
3) The Park transformation requirement to implement the control scheme is eliminated and reduces the mathematical computation burden
4) Inclusion of estimated parameters from the observer structure to reduce the noise and gain drift in measured parameters due to sensors

This paper is organized as follows. Section II explains the mathematical model of the five-phase IPMSM. In section III, a brief description of observer structure is given. Section IV describes the classical control structure for five-phase IPMSM. In Section V, the proposed control structure is explained in detail. Section VI represents simulation and experimental results, followed by a conclusion in Section VII.

II. MATHEMATICAL MODEL OF IPMSM

The mathematical model of a five-phase IPMSM can be prepared similarly to a three-phase machine. However, due to the higher number of phases, it requires certain adjustments. The natural reference frame of five-phase IPMSM (a-b-c-d-e) can be transformed into two independent stationary orthogonal planes: the fundamental (α_1-β_1) and the third harmonic (α_2-β_2), respectively. The mathematical structure of five-phase IPMSM is well known in the literatures [20], [21], and [22]. In a stationary reference frame, a vector model of five-phase IPMSM for the fundamental plane and the second plane can be presented in the form of differential equations as follows:

$$\frac{\mathrm{d}i_{s\alpha(i)}}{\mathrm{d}\tau} = -\frac{1}{L_{q(i)}}R_s i_{s\alpha(i)} + \frac{1}{L_{q(i)}}\omega_{r(i)}\psi_{f\beta(i)} + \frac{1}{L_{q(i)}}u_{s\alpha(i)} \quad (1)$$

$$\frac{\mathrm{d}i_{s\beta(i)}}{\mathrm{d}\tau} = -\frac{1}{L_{q(i)}}R_s i_{s\beta(i)} - \frac{1}{L_{q(i)}}\omega_{r(i)}\psi_{f\alpha(i)} + \frac{1}{L_{q(i)}}u_{s\beta(i)} \quad (2)$$

$$\frac{\mathrm{d}\omega_{r(i)}}{\mathrm{d}\tau} = \frac{1}{J}\left(\sum_{i=1}^{N}(\psi_{\alpha(i)}i_{s\beta(i)} - \psi_{\beta(i)}i_{s\alpha(i)}) - T_L\right) \quad (3)$$

$$\frac{\mathrm{d}\theta_{r(i)}}{\mathrm{d}\tau} = \omega_{r(i)} \quad (4)$$

where $i = 1$ and 2, $\boldsymbol{i}_{s(i)}$, $\boldsymbol{u}_{s(i)}$, $\boldsymbol{\psi}_{s(i)}$, and $\boldsymbol{\psi}_{f(i)}$ are the vectors representing fundamental and third harmonic stator current, stator voltage, stator flux and permanent flux components. Rs is stator resistance, $L_{q(i)}$ is stator inductance, load torque is T_L, and system inertia is J. It is assumed that the parameters of the five-phase IPMSM are known and constant. The next section discusses the adaptive observer structure in brief detail.

III. OBSERVER STRUCTURE OF FIVE-PHASE IPMSM

Based on the mathematical model of five-phase IPMSM, observer structure in $\alpha_{(i)}$-$\beta_{(i)}$ coordinates can be prepared as:

$$\frac{\mathrm{d}\hat{i}_{s\alpha(i)}}{\mathrm{d}\tau} = -\frac{1}{L_{q(i)}}R_s\hat{i}_{s\alpha(i)} + \frac{1}{L_{q(i)}}\hat{\omega}_{(i)}\hat{\psi}_{f\beta(i)} + \frac{1}{L_{q(i)}}u_{s\alpha(i)} + v_{\alpha(i)} \quad (5)$$

$$\frac{\mathrm{d}\hat{i}_{s\beta(i)}}{\mathrm{d}\tau} = -\frac{1}{L_{q(i)}}R_s\hat{i}_{s\beta(i)} - \frac{1}{L_{q(i)}}\hat{\omega}_{(i)}\hat{\psi}_{f\alpha(i)} + \frac{1}{L_{q(i)}}u_{s\beta(i)} + v_{\beta(i)} \tag{6}$$

$$\frac{\mathrm{d}\hat{\theta}_{(i)}}{\mathrm{d}\tau} = \hat{\omega}_{(i)} \tag{7}$$

$$\hat{\psi}_{f\alpha(i)} = \psi_{f(i)}\cos\hat{\theta}_{r(i)} \tag{8}$$

$$\hat{\psi}_{f\beta(i)} = \psi_{f(i)}\sin\hat{\theta}_{r(i)} \tag{9}$$

Estimated state variables in the observer structure are represented by "^". Input voltage vector components are $u_{s\alpha(i)}$ and $u_{s\beta(i)}$, $\hat{i}_{s\alpha(i)}$ and $\hat{i}_{s\beta(i)}$, are estimated current vector components, $\hat{\psi}_{f\alpha(i)}$ and $\hat{\psi}_{f\beta(i)}$ represents flux components calculated using estimated angular position, $v_{\alpha(i)}$ and $v_{\beta(i)}$ are added stabilizing functions to make the observer structure asymptotically stable. The final form of the stabilizing functions can be obtained using the Lyapunov stability theorem. The error between the estimated value and the measured value can be calculated using (10)

$$\tilde{i}_{s\alpha,\beta(i)} = \hat{i}_{s\alpha,\,\beta(i)} - i_{s\alpha,\beta(i)},\ \tilde{\omega}_{r(i)} = \hat{\omega}_{r(i)} - \omega_{r(i)},\quad \tilde{\theta}_{r(i)} = \hat{\theta}_{r(i)} - \theta_{r(i)}, \tag{10}$$

Rotor speed values for the first and second planes can be estimated from (11).

$$\dot{\hat{\omega}}_{r(i)} = -\gamma_{(i)}(\hat{\psi}_{f\beta(i)}\tilde{i}_{s\alpha(i)} - \hat{\psi}_{f\alpha(i)}\tilde{i}_{s\beta(i)})\text{for}\gamma > 0\text{and}\dot{\tilde{\omega}}_{r(i)} \approx \dot{\hat{\omega}}_{r(i)} \tag{11}$$

This article is focused on the proposed control scheme for five-phase IPMSM; hence, the discussion on observer structure is limited. The next section discusses the classical control scheme where MPC-based FOC is used for the first plane and PI controller-based FOC for the second plane.

IV. CLASSICAL CONTROL SCHEME OF FIVE-PHASE IPMSM

For control of five-phase IPMSM, the traditional control schemes: MPC for the fundamental plane, which is also known as traditional PTC, and PI controller-based FOC for 3rd harmonic plane is shown in Fig. 1. In the fundamental plane, the PI controller is implemented for accurate speed control and produce reference current for $i^*_{sq(1)}$. For sampling time T_s, the derivative of stator currents can be approximated using Euler approximation, and the final form of predictive currents model in the rotating reference frame can be obtained, based on the voltage vectors generated by the inverter in the stationary reference frame are the rotating vectors in *(d-q)* reference frame and stator currents can be predicted, which is well known in the literature [7]. The predictive current controller tracks the reference current generated by the PI controller. The voltage vector, which minimizes the defined cost function in (12) will be applied for the whole sampling period [11].

$$g = ((i^*_{sd(i)} - i^{\mathrm{P}(k+1)}_{sd(i)}) + (i^*_{sq(i)} - i^{\mathrm{P}(k+1)}_{sq(i)}))^2 \tag{12}$$

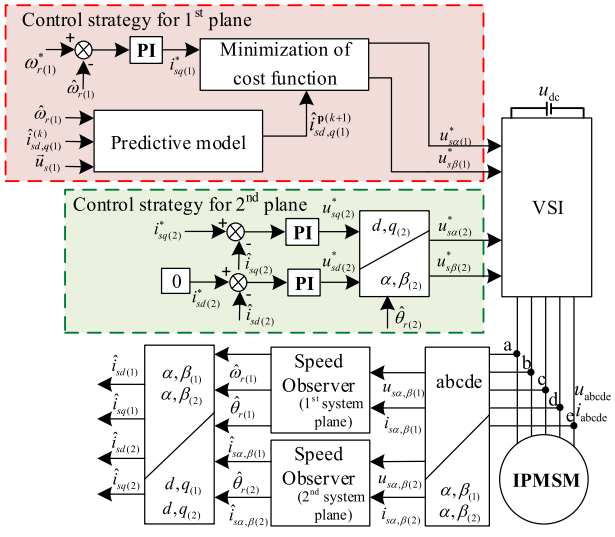

FIGURE 1. The control diagram of classical predictive current control based FOC for 1st plane and classical FOC for 2nd plane.

In the second plane, PI controllers control the flux and torque components of the currents. In the second plane, the reference current $i^*_{sq(2)}$ is calculated optimally from the fundamental reference current $i^*_{sq(1)}$ [6].

In the control scheme, measured currents and voltages in the natural reference frame are transformed into the stationary reference frame to implement the observer structure. The observer structure estimates the defined state variables in the stationary reference frame. State variables are converted into the rotating reference frame for control system implementation using an estimated angular position. To implement the classical control structure for the five-phase IPMSM drive, it is necessary to transform state variables in $(d\text{-}q)$ reference frame as shown in Fig. 1.

V. PROPOSED CONTROL SCHEME OF FIVE-PHASE IPMSM

A. PROPOSED PREDICTIVE CONTROL OF MULTI-SCALAR VARIABLES FOR FUNDAMENTAL PLANE

The conceptualization behind the multi-scalar is that the inner and external product of the stator current vector ($\boldsymbol{i}_{s(i)}$) and stator flux vector ($\boldsymbol{\psi}_{s(i)}$) can be transformed into scalars [3], [23]. For the fundamental plane $\boldsymbol{i} = 1$, in the nonlinear control such as five-phase IPMSM, these four are state variables in each plane

$$x_{11(i)} = \omega_{r(i)} \tag{13}$$

$$x_{12(i)} = \psi_{s\alpha(i)}i_{s\beta(i)} - \psi_{s\beta(i)}i_{s\alpha(i)} \tag{14}$$

$$x_{21(i)} = \psi^2_{s\alpha(i)} + \psi^2_{s\beta(i)} \tag{15}$$

$$x_{22(i)} = \psi_{s\alpha(i)}i_{s\alpha(i)} + \psi_{s\beta(i)}i_{s\beta(i)} \tag{16}$$

$\mathrm{x}_{11(i)}$ is rotor speed, $\mathrm{x}_{12(i)}$ is an external product of stator flux and current which represents the motor torque, $\mathrm{x}_{21(i)}$ is the square of stator flux, and $\mathrm{x}_{22(i)}$ is the inner product of stator flux and stator currents. The proposed control strategy for five-phase IPMSM is depicted in Fig. 2.

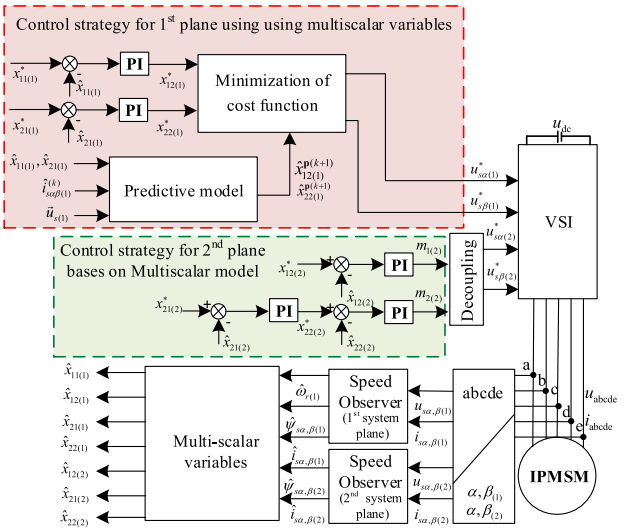

FIGURE 2. The control diagram of the proposed predictive control using multi-scalar variables for 1st plane and multi-scalar model-based control for 2nd plane.

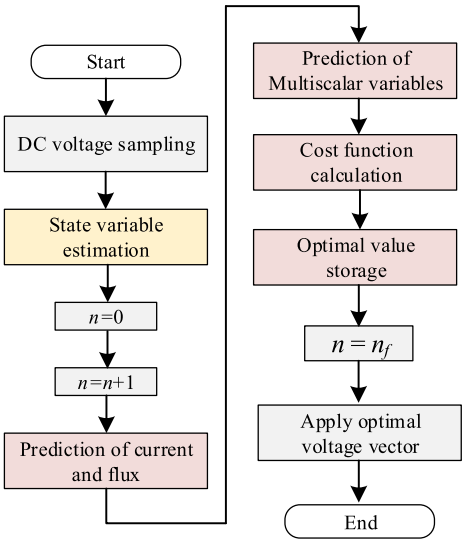

FIGURE 3. Flowchart of the proposed control diagram of proposed predictive control using multi-scalar variables for 1st plane.

The control objective is prepared for the fundamental plane based on multi-scalar variables. Predictive control is employed to control the multi-scalar variables. Multi-scalar model-based control is proposed for 2nd plane to control the flux and torque components. It can be observed from Fig. 2. that park transformation is not required in the second plane to control the third harmonic components.

To discretize the (1) and (2), the forward Euler method can be used, and the stator current at instant (k + 1) can be predicted as:

$$i_{s\alpha(i)}^{(k+1)} = (1 - \frac{T_s}{T_{v(i)}})i_{s\alpha(i)}^{(k)} + \frac{T_s}{L_{q(i)}}\omega_{r(i)}\psi_{f\beta(i)} + \frac{T_s}{L_{q(i)}}u_{sa(i)}^{(k)} \tag{17}$$

$$i_{s\beta(i)}^{(k+1)} = (1 - \frac{T_s}{T_{v(i)}})i_{s\beta(i)}^{(k)} - \frac{T_s}{L_{q(i)}}\omega_{r(i)}\psi_{f\alpha(i)} + \frac{T_s}{L_{q(i)}}u_{s\beta(i)}^{(k)} \tag{18}$$

where $T_{v(i)} = \frac{L_{q(i)}}{R_s}$.

Based on (17) and (18) the predicted current value, stator flux can be predicted for the same current vector

$$\psi_{s\alpha(i)}^{(k+1)} = (L_{q(i)}i_{s\alpha(i)}^{(k)} + \psi_{f\alpha(i)}) \tag{19}$$

$$\psi_{s\beta(i)}^{(k+1)} = (L_{q(i)}i_{s\beta(i)}^{(k)} + \psi_{f\beta(i)}) \tag{20}$$

After substituting the predicted value of stator currents and stator flux in (14) and (16), multi-scalar variables: $x_{12(i)}$ which represents torque, and $x_{22(i)}$ which is the reactive component of torque, can also be predicted and given as

$$x_{12(i)}^{(k+1)} = \psi_{s\alpha(i)}^{(k+1)}i_{s\beta(i)}^{(k+1)} - \psi_{s\beta(i)}^{(k+1)}i_{s\alpha(i)}^{(k+1)} \tag{21}$$

$$x_{22(i)}^{(k+1)} = \psi_{s\alpha(i)}^{(k+1)}i_{s\alpha(i)}^{(k+1)} + \psi_{s\beta(i)}^{(k+1)}i_{s\beta(i)}^{(k+1)} \tag{22}$$

The unit and dimension of (21) and (22) are the same; hence, the weighting factor can be eliminated, and the following cost function is proposed in this article.

$$g = ((x_{12(i)}^{*} - x_{12(i)}^{P(k+1)}) + (x_{22(i)}^{*} - x_{22(i)}^{P(k+1)}))^2 \tag{23}$$

The reference value of torque $x_{12(1)}^{*}$ is generated using a speed controller, and the reference value of reactive torque $x_{22(1)}^{*}$ is obtained from the flux controller $x_{21(1)}^{*}$. In the proposed scheme, the value of stator flux is kept constant, hence $x_{22(i)} \neq 0$ for the proposed control scheme. Following the above procedure, a predictive controller can be designed for the fundamental plane of the five-phase IPMSM, as shown in the red dashed box in Fig. 2. At the instant of k, estimated current signals from the adaptive observer are used instead of measured current signals. Implementing multi-scalar variable-based PTC does not require angle transformation.

It is important to mention that in the proposed control solution, measure speed $\omega_{r(i)}$, position $\theta_{r(i)}$, permanent magnet flux components $\psi_{f\alpha,\beta(i)}$, stator flux components $\psi_{s\alpha,\beta(i)}$, and stator current components $i_{s\alpha,\beta(i)}$ are replaced with estimated speed $\hat{\omega}_{r(i)}$, position $\hat{\theta}_{r(i)}$, permanent magnet flux components $\hat{\psi}_{f\alpha,\beta(i)}$, stator flux components $\hat{\psi}_{s\alpha,\beta(i)}$ and stator current components $\hat{i}_{s\alpha,\beta(i)}$ for fundamental plane and second plane to avoid the issue of noise and gain drift due to mechanical sensor. It is assumed that machine parameters are known and constant in nature. The flowchart of the proposed PTC based on multi-scalar variables is shown in Fig. 3.

B. PROPOSED MULTI-SCALAR CONTROL FOR THE SECOND PLANE

This article proposes a multi-scalar model-based control for the third harmonic component in the second plane for five-phase IPMSM. For the second plane, $i = 2$. By taking the time derivative of multi-scalar variables (13)-(16), the multi-scalar model of the nonlinear control system can be

prepared as (24)-(27).

$$\frac{dx_{11(i)}}{dt} = \frac{1}{J}x_{12(i)} - \frac{1}{J}T_L \tag{24}$$

$$\frac{dx_{12(i)}}{dt} = -\frac{1}{T_{v(i)}}x_{12(i)} - \frac{1}{L_{q(i)}}x_{11(i)}(\psi_{s(i)} \odot \psi_{f(i)}) + q_{s(i)} + \underbrace{\frac{1}{L_{q(i)}}(\psi_{s\alpha(i)}u_{s\beta(i)} - \psi_{s\beta(i)}u_{s\alpha(i)})}_{u_{1(i)}} \tag{25}$$

$$\frac{dx_{21(i)}}{dt} = 2(-R_s x_{22(i)} + u_{s\alpha(i)}\psi_{s\alpha(i)} + u_{s\beta(i)}\psi_{s\beta(i)}) \tag{26}$$

$$\frac{dx_{22(i)}}{dt} = -\frac{1}{T_{v(i)}}x_{22(i)} - R_s i^2_{s(i)} + \frac{1}{L_{q(i)}}x_{11(i)}(\psi_{s(i)} \otimes \psi_{f(i)}) + p_{s(i)} + \underbrace{\frac{1}{L_{q(i)}}(\psi_{s\alpha(i)}u_{s\alpha(i)} + \psi_{s\beta(i)}u_{s\beta(i)})}_{u_{2(i)}} \tag{27}$$

where $T_{v(i)}$ is the motor electromagnetic time constant and additional terms appearing from (25) to (27) are expressed as:

$$T_{v(i)} = \frac{L_{q(i)}}{R_s} \tag{28}$$

$$(\psi_{s(i)} \odot \psi_{f(i)}) = (\psi_{s\alpha(i)}\psi_{f\alpha(i)} + \psi_{s\beta(i)}\psi_{f\beta(i)}) \tag{29}$$

$$(\psi_{s(i)} \otimes \psi_{f(i)}) = (\psi_{s\alpha(i)}\psi_{f\beta(i)} - \psi_{s\beta(i)}\psi_{f\alpha(i)}) \tag{30}$$

$$p_{s(i)} = u_{s\alpha(i)}i_{s\alpha(i)} + u_{s\beta(i)}i_{s\beta(i)} \tag{31}$$

$$q_{s(i)} = u_{s\alpha(i)}i_{s\beta(i)} - i_{s\alpha(i)}u_{s\beta(i)} \tag{32}$$

$$i^2_{s(i)} = (i^2_{s\alpha(i)} + i^2_{s\beta(i)}) \tag{33}$$

In the following step, feedback linearization process must be completed. New signals $m_{1(i)}$ and $m_{2(i)}$ are computed using PI controller to linear the nonlinear systems as shown green dashed box in Fig. 2. To generate PWM signals, reference voltage components are required, and it can be obtained from multi-scalar control signal:

$$u_{s\alpha(i)} = L_{q(i)}\left(\frac{u_{2(i)}\psi_{sa(i)} - u_{1(i)}\psi_{s\beta(i)}}{x_{21(i)}}\right) \tag{34}$$

$$u_{s\beta(i)} = L_{q(i)}\left(\frac{u_{2(i)}\psi_{s\beta(i)} + u_{1(i)}\psi_{s\alpha(i)}}{x_{21(i)}}\right) \tag{35}$$

It can be observed that after the completing process of linearization and decoupling two linear subsystems are obtained: mechanical subsystem expressed in (36) and (37) and electromagnetic subsystem expressed in (38) and (39).

$$\frac{dx_{11(i)}}{dt} = \frac{1}{J}x_{12(i)} - \frac{1}{J}T_L \tag{36}$$

$$\frac{dx_{12(i)}}{dt} = -\frac{1}{T_{v(i)}}x_{12(i)} + m_{1(i)} \tag{37}$$

$$\frac{dx_{21(i)}}{dt} = 2(-R_s x_{22(i)} + u_{s\alpha(i)}\psi_{s\alpha(i)} + u_{s\beta(i)}\psi_{s\beta(i)}) \tag{38}$$

$$\frac{dx_{22(i)}}{dt} = -\frac{1}{T_{v(i)}}x_{22(i)} + m_{2(i)} \tag{39}$$

Control structure based on $(d-q)$ coordinates, requires additional transformation of state variables from stationary reference frame $(\alpha\text{-}\beta)$ to synchronous reference frame $(d-q)$. It can be seen from Fig. 2, the proposed control scheme is based on stationary reference frame $(\alpha\text{-}\beta)$, and the Park transformation $(d-q)$ requirement to implement the control scheme is eliminated which reduces the mathematical computation burden. Moreover, the classical control fails to decouple the system completely in the presence of nonlinearity due to the machine state variable transformation to the rotating reference frame (d-q) strongly discussed in [24] and [25]. The proposed control scheme provides proper decoupling of nonlinear machine model in $(\alpha\text{-}\beta)$ reference frame based on chosen variables: scalar and vector product of stator current and stator flux.

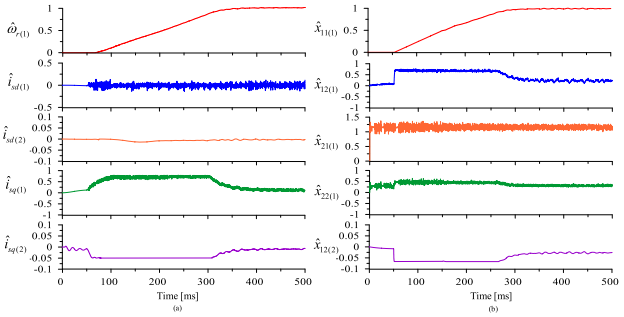

FIGURE 4. Simulation results of the machine starting up to nominal speed a) classical control scheme b) proposed control scheme.

VI. SIMULATION AND EXPERIMENTAL RESULTS

A. SIMULATION RESULTS

The effectiveness of the proposed control structure is verified using simulation and experimental results. In Fig. 4. the chosen simulation results are presented. The IPMSM is starting up to nominal speed to confirm the theoretical hypothesis.

In Fig. 4 a), classical control scheme performance is shown with estimated speed $\hat{\omega}_{r(1)}$, estimated flux controlling current $\hat{i}_{sd(1)}$, $\hat{i}_{sd(2)}$ and torque controlling current $\hat{i}_{sq(1)}$, $\hat{i}_{sq(2)}$ for fundamental plane and second plane. In Fig. 4 b), simulation result of the proposed control scheme is shown. Multi-scalar variables: estimated rotor speed $\hat{x}_{11(1)}$, generated electromagnetic torque $\hat{x}_{12(1)}$ and reactive torque components $\hat{x}_{22(1)}$, square of stator flux torque $\hat{x}_{21(1)}$ in first plane and generated electromagnetic torque $\hat{x}_{12(2)}$ in second plane are shown.

B. EXPERIMENTAL RESULTS

In order to evaluate the behaviour of the proposed control scheme in real-time operating conditions, the presented control system was precisely verified by the use of a set of laboratory equipment. The laboratory set employed 5.5 kW five-phase IPMSM drive system supplied by the VSC. Parameters of the electric drive system are given in Table. 1. DSP sharc ADSP21363 floating-point signal processor and Altera Cyclone 2 FPGA are used in the interface for control system implementation. The switching frequency of the transistor was 3.3kHz. 150 μs were chosen as the sample time duration. In Fig. 1 and Fig.2, control system structures in the DSP board are shown. Current measurement was done using LA 25-NP

TABLE 1. IPMSM parameters and reference unit.

Symbol	Quantity	Values
R_{sn}	stator resistance	0.816 Ω / 0.0680 p.u.
$L_{dn(1)}$	$d_{(1)}$-axis inductance	10.85 mH / 0.4263 p.u.
$L_{dn(2)}$	$d_{(2)}$-axis inductance	3.61 mH / 0.1421 p.u.
$L_{qn(1)}$	$q_{(1)}$-axis inductance	16.5 mH / 0.6484 p.u.
$L_{qn(2)}$	$q_{(2)}$-axis inductance	5.5 mH / 0.2161 p.u.
P	pole pairs	3
P_n	nominal power	5.5 kW
T_{en}	nominal value of torque	35.0 Nm / 0.8817 p.u.
$\psi_{f(1)}$	permanent magnets flux linkage $_{(1)}$	0.51 Wb / 0.89 p.u.
$\psi_{f(2)}$	permanent magnets flux linkage $_{(2)}$	0.040 Wb / 0.07 p.u.
U_n	nominal stator voltage (Y)	275 V
I_n	nominal stator current (Y)	10.2 A
n	nominal rotor speed	1500 rpm
f	nominal frequency	75 Hz
U_b=Un	reference voltage	275 V
I_b=In√5	reference current	22.80 A

TABLE 2. Tuning gains of the classical control structure.

Symbol	Controller	Gains
$k_{p\omega(1)}$	proportional gain for speed$_{(1)}$ controller	5
$k_{i\omega(1)}$	integral gain for speed$_{(1)}$ controller	0.02
$k_{pid(2)}$	proportional gain for $d_{(2)}$-axis current controller	3.5
$k_{iid(2)}$	integral gain for $d_{(2)}$-axis current controller	0.1
$k_{piq(2)}$	proportional gain for $q_{(2)}$-axis current controller	2
$k_{iiq(2)}$	integral gain for $q_{(2)}$-axis current controller	0.1

TABLE 3. Tuning gains of the proposed control structure.

Symbol	Controller	Gains
$k_{px11(1)}$	proportional gain for $x_{11(1)}$ controller	10
$k_{ix11(1)}$	integral gain for $x_{11(1)}$ controller	0.02
$k_{px21(1)}$	proportional gain for $x_{21(1)}$ controller	1
$k_{ix21(1)}$	integral gain for $x_{21(1)}$ controller	0.1
$k_{px12(2)}$	proportional gain for $x_{12(2)}$ controller	5
$k_{ix12(2)}$	integral gain for $x_{12(2)}$ controller	0.1
$k_{px21(2)}$	proportional gain for $x_{21(2)}$ controller	1.5
$k_{ix21(2)}$	integral gain for $x_{21(2)}$ controller	0.1
$k_{px22(2)}$	proportional gain for $x_{22(2)}$ controller	5
$k_{ix22(2)}$	integral gain for $x_{22(2)}$ controller	0.1

current transducers, and later on transformed to the stationary reference frame (α-β) using the Clark transformation. Rotational speed was measured using the incremental encoder (11-bits). The only purpose of using the encoder was to verify the estimation accuracy of the observer structure. Controller tuning gains used for experimental tests for classical and proposed control schemes are given in Table. 2 and Table. 3.

1) DRIVE STARTING AND REVERSAL

The first scenario is presented in the Fig. 5 where the machine is starting up to 1.0 p.u. at no-load during this test. In Fig. 5 a) measured speed $\omega_{r(i)}$, estimated speed $\hat{\omega}_{r(1)}$, speed estimation error $\tilde{\omega}_{r(1)}$, generated torque in first plane $\hat{i}_{sq(1)}$, and second plane $\hat{i}_{sq(2)}$ are shown for classical control scheme and in Fig. 5 b), measured speed $x_{11(1)}$, estimated rotor speed $\hat{x}_{11(1)}$,

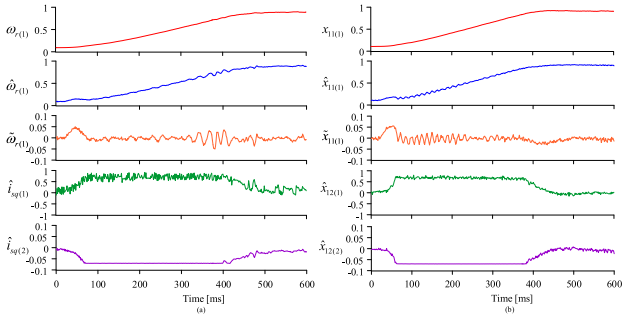

FIGURE 5. Experimental results of machine starting up to nominal speed a) classical control scheme b) proposed control scheme.

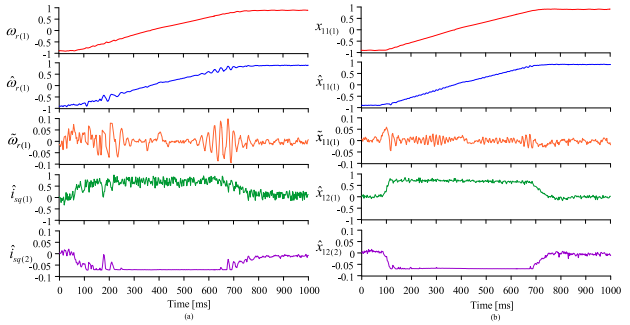

FIGURE 6. Experimental results of machine reversing from −1.0 to 1.0 p.u. a) classical control scheme b) proposed control scheme.

speed estimation error $\tilde{x}_{11(1)}$, torque representing quantities $\hat{x}_{12(1)}, \hat{x}_{12(2)}$ for fundamental and third harmonic plane are shown for the proposed control scheme. The estimated speed error between the measured speed and estimated speed is less than 0.05 p.u.

In Fig. 5, during the transient state, torque reaches a maximum limit of 0.7 for the first plane and 0.07 for the second plane and goes to zero when the motor reaches a steady state. The torque provided by the first and second planes during the dynamic state in both control structures is almost the same as the simulation results, confirming the theoretical hypothesis.

In Fig. 6, the five-phase IPMSM reverses from −1.0 to 1.0 p.u. at no-load using the estimated rotor speed. Fig 6 a), shows the performance of the classical control scheme and Fig. 6 b), depicts the performance of the proposed control scheme. In Fig. 6 a), the speed estimation error during the dynamic state is close to 0.1 p.u. while in Fig. 6 b), it remains under 0.05 p.u. using the proposed control structure. The maneuver corresponds to speed reversal using the proposed PTC, introducing less distortion in the torque than classical PTC. During the dynamic state, the torque generated in the second plane by the third harmonic current injection is almost 10% of the fundamental torque. Moreover, without using the weighting factor, proposed control scheme provides a better dynamic response than the classical control scheme.

In Fig. 7 a), five-phase IPMSM drive is starting up to nominal speed and in Fig. 7 b) five-phase IPMSM drive is reversing from 1.0 p.u. to −1.0 p.u. using the proposed control solution. Multiscalar variables: estimated speed $\hat{x}_{11(1)}$, square of stator flux $\hat{x}_{21(1)}$, reactive torque component $\hat{x}_{22(1)}$

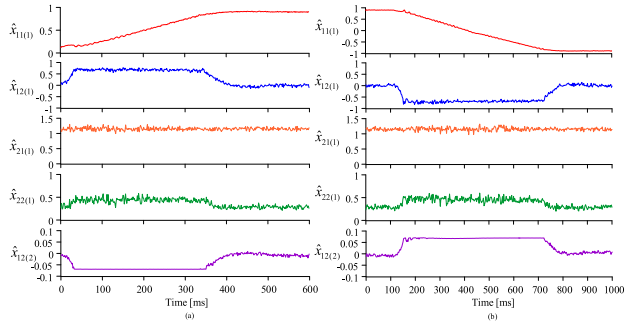

FIGURE 7. Experimental results of five-phase IPMSM a) starting up to 1.0 p.u. and b) reversing from 1.0 to −1.0 p.u. using the proposed control scheme.

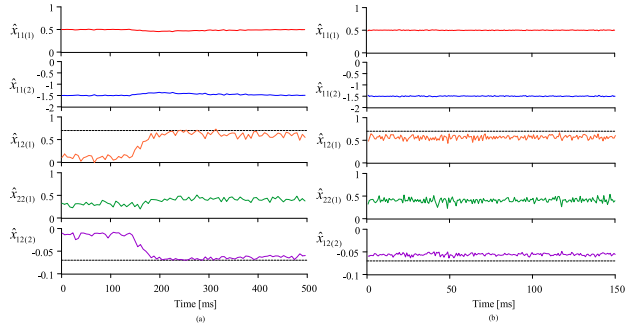

FIGURE 8. Experimental results of loaded five-phase IPMSM a) after 0.13 s the load torque was changed from 0.1 to 0.6 p.u. and b) stationary state is presented in 150 ms period.

of first plane and generated electromagnetic torque in first plane $\hat{x}_{12(1)}$ and second plane $\hat{x}_{12(2)}$ are show in Fig. 7 a) and Fig. 7 b). In this control scheme, the square of state flux $\hat{x}_{21(1)}$ defined in (15) is kept constant. To maintain a constant value of the square of stator flux in five-phase IPMSM for the first plane, $\hat{x}_{22(1)}$ has to be positive, which can be seen for both cases: machine starting up to nominal speed and reversing from 1.0 to −1.0 p.u.

From Fig. 7, to keep the flux level constant, the demand $\hat{x}_{22(1)}$ is less during steady-state conditions, but during dynamic conditions, the requirement of $\hat{x}_{22(1)}$ increases. Torque components for the first and second planes $\hat{x}_{12(2)}$ are also shown for both cases.

2) LOAD TORQUE INJECTIONS FOR MEDIUM SPEED

In the second scenario, the rotor speed was set to 0.5 p.u. and the applied load torque was 0.1 p.u. After 0.13 s, load torque was increased to $T_L = 0.6$ p.u. To conduct the test, torque variables $\hat{x}_{12(1)}$ was limited to 0.7 and $\hat{x}_{12(2)}$ to 0.07, respectively. In Fig. 8 a) estimated rotor speed for first plane $\hat{x}_{11(1)}$ and second plane $\hat{x}_{11(2)}$, torque variables of both plane, and reactive torque component of first plane $\hat{x}_{22(1)}$, are displayed.

Fig. 8 a) presents when applied load torque was changed from 0.1 p.u. to 0.6 p.u., the demand of reactive torque $\hat{x}_{22(1)}$ also increased to maintain constant level of stator flux $\hat{x}_{21(1)}$. In Fig. 8 b), steady state performance of the five-phase IPMSM drive is presented for the same working points for the period of 150ms. It can be seen that at steady state, estimated speed of first plane $\hat{x}_{11(1)}$ was maintained at 0.5 p.u. and

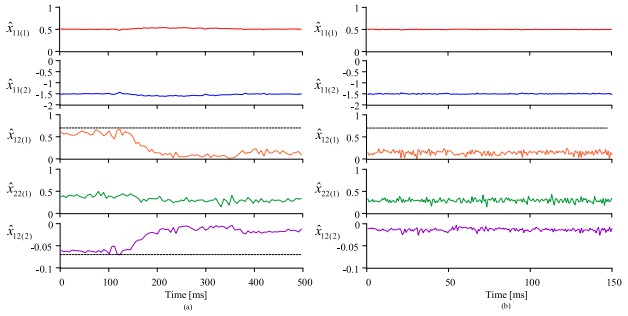

FIGURE 9. Experimental results of loaded five-phase IPMSM a) after 0.1 s the load torque was changed from 0.6 to 0.1 p.u. and b) stationary state is presented in 150 ms period.

estimated speed of second plane $\hat{x}_{11(2)}$ was maintained at −1.5 p.u. Moreover, generated electromagnetic torque in first plane $\hat{x}_{12(1)}$ and second plane $\hat{x}_{12(2)}$ were around 0.6 p.u. and 0.06 p.u., respectively. Demand of reactive torque $\hat{x}_{22(1)}$ also increased from 0.25 p.u. and settled at 0.45 p.u to keep the stator flux at desired level.

Fig. 9 shows the dynamic and steady-state performance of the five-phase IPMSM when the load is reduced. In Fig. 9 a), the rotor was rotating at a reference speed of 0.5 p.u. for the first plane and 0.6 p.u. load was connected. After 0.1 s, load was reduced to 0.1 p.u. Due to the sudden reduction in load, speed increases for a very small time and again reaches the reference speed, and torque value settles at the desired value. The requirement of reactive torque components to maintain stator flux level also reduced as the applied load is reduced. Steady-state performance for the same working points is visible in Fig. 9 b) for the small period of 150 ms. As shown in Fig. 9 b), estimated speed was maintained at defined value, electromagnetic torque supplied by five-phase IPMSM for fundamental plane $\hat{x}_{12(1)}$ was around 0.1 p.u. and for second plane $\hat{x}_{12(2)}$ was around 0.01 p.u. Reactive torque $\hat{x}_{22(1)}$ demand was reduced upto 0.25 p.u. in steady state. From Fig. 8 and Fig. 9, The proposed control solution remains stable and provides fast dynamic response in the case of load injection and load removal.

3) LOW SPEED OPERATION AND STANDSTILL TEST

In Fig. 10 a), IPMSM drive reverses under load torque, $T_L = -0.2$ p.u. Performance of observer structure and proposed control scheme is good during low speed reversal. Fundamental speed $\hat{x}_{11(1)}$ reverses from 0.1 to −0.1 p.u. and speed of second plane $\hat{x}_{11(2)}$ reverses from −0.3 to 0.3 p.u. Flux level $\hat{x}_{21(1)}$ is maintained constant at 1.15 p.u. for the first plane. When the machine is in a transient state, the supplied electromagnetic torque changes $\hat{x}_{12(1)}, \hat{x}_{12(2)}$ from −0.2 p.u. and 0.02 p.u. to maximum allowable limit −0.7 p.u. and 0.07 p.u., respectively, and when the reversal is completed to −0.1, the torque value again approaches −0.2 p.u. and 0.02 p.u. Fig. 11 b), shows standstill test for five-phase IPMSM drive. The rotor speed is switched from 0.3 to 0 p.u. for 1.8 s and again to 0.3 p.u. after 2.2 s. This test shows that the IPMSM successfully comes back to the set reference speed of 0.3 p.u. without getting stuck at zero speed and losing synchronism.

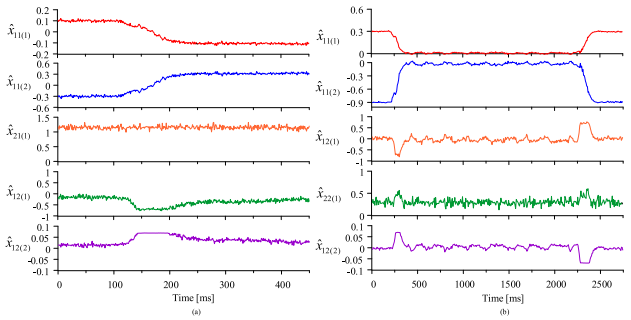

FIGURE 10. Experimental results of five-phase IPMSM a) rotor speed is changed from 0.1 to −0.1 p.u. with load −0.2 p.u. and b) machine standstill test without load.

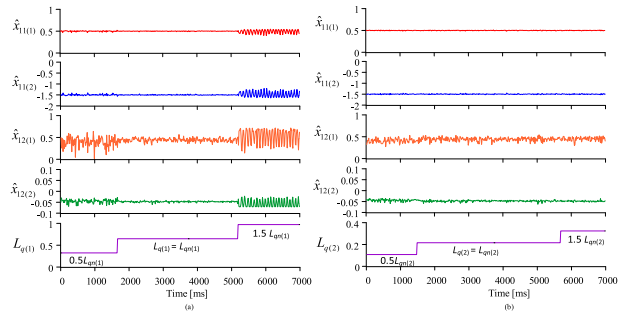

FIGURE 11. Experimental results of five-phase IPMSM loaded at about 0.45 p.u. of load torque, rotor speed is 0.5 p.u. for different value of inductances a) $L_{q(1)}$ b) $L_{q(2)}$.

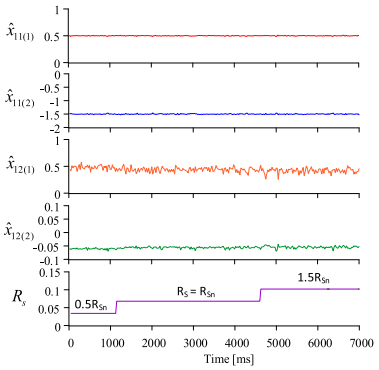

FIGURE 12. Experimental results of five-phase IPMSM loaded at about 0.45 p.u. of load torque, rotor speed is 0.5 p.u. for different values of resistance.

4) UNCERTAINTY OF MACHINE PARAMETERS

In Fig. 11, the test of the robustness of the proposed control system on the changes of the nominal values of inductances $L_{q(1)}$ and $L_{q(2)}$ of five-phase IPMSM is presented. The reference speed of the rotor was set at 0.5 p.u. and the value of load torque, $T_L = 0.45$ p.u. In Fig. 11 a), $L_{q(1)}$ was $0.5L_{qn(1)}$ and after 1.7 s $L_{q(1)} = L_{qn(1)}$ and after 5.7s $L_{q(1)} = 1.5\ L_{qn(1)}$. In Fig. 11 b), the same working points are implemented for various values of the second plane's inductance $L_{q(2)}$. In Fig 11. b), The second plane control system is robust and maintains the system's stability on changes in the value of inductance $L_{q(2)}$; however, when the value of inductance of the first plane changes to $L_{q(1)} = 1.5\ L_{qn(1)}$, the stability of the system reduces.

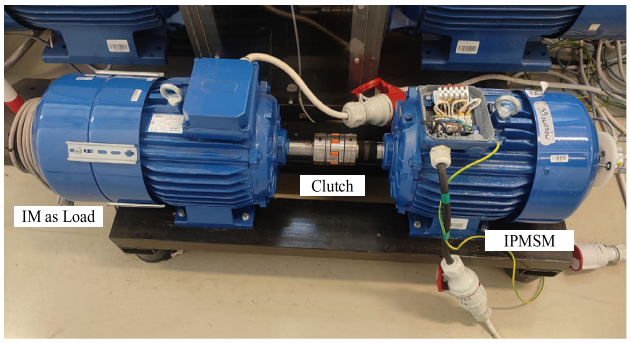

FIGURE 13. Photograph of the experimental stand with the IPMSM clutched to induction machine.

In Fig. 12, the value of resistance changed in three stages: $R_s = 0.5R_{sn}$, $R_s = R_{sn}$ and $R_s = 1.5R_{sn}$. The rotor speed was set at 0.5 p.u. and the machine was loaded at about 0.45 p.u. The control system proves to be robust and stable against the changes of different resistance values as shown in the Fig. 12.

VII. CONCLUSION

This paper presents a new control structure for five-phase IPMSM. Fundamental components are in the first plane and controlled by the predictive control of multi-scalar variables. Third harmonics components are in the second plane and controlled by the multi-scalar control scheme. The proposed control scheme for both planes is in the α-β reference frame, simplifying the control structure and reducing the processor's mathematical burden. In the classical control scheme, the Park transformation is needed to implement the control scheme, which increases overall computation time and increases the complexity of the system. The proposed control scheme of the first and second planes was compared with the classical PTC for the first plane and classical FOC for the second plane for the case of the machine starting up to nominal speed and reversal. The performance of the proposed control structure is more adequate and introduces less distortion in the electromagnetic torque compared to the classical control structure. Moreover, in this article, the use of the weighting factor for predictive control was eliminated without degrading the performance of the control structure. Both the simulation and experimental results validate that the performance of the proposed control structure is stable. The proposed control scheme presented in this article was tested for four different scenarios. The obtained results by the experimental implementation confirmed the excellent performance of the proposed control structure for five-phase IPMSM.

REFERENCES

[1] E. Levi, F. Barrero, and M. J. Duran, "Multiphase machines and drives—Revisited," *IEEE Trans. Ind. Electron.*, vol. 63, no. 1, pp. 429–432, Jan. 2016, doi: 10.1109/TIE.2015.2493510.
[2] S. Rubino, O. Dordevic, E. Armando, I. R. Bojoi, and E. Levi, "A novel matrix transformation for decoupled control of modular multiphase PMSM drives," *IEEE Trans. Power Electron.*, vol. 36, no. 7, pp. 8088–8101, Jul. 2021, doi: 10.1109/TPEL.2020.3043083.
[3] B. M. Wilamowski and J. D. Irwin, "Power electronics and motor drives (The industrial electronics handbook)," Tech. Rep., 2011.
[4] L. Parsa and H. A. Toliyat, "Five-phase permanent-magnet motor drives," *IEEE Trans. Ind. Appl.*, vol. 41, no. 1, pp. 30–37, Jan. 2005, doi: 10.1109/TIA.2004.841021.

[5] J. Zhang, S. J. He, and K. Wang, "Multi-harmonic currents control strategy for five-phase permanent magnet machine with non-sinusoidal back-EMF," *IEEE Access*, 2020, doi: 10.1109/ACCESS.2020.2989323.

[6] J. Li, B. Du, T. Zhao, Y. Cheng, and S. Cui, "Third-harmonic current injection control of five-phase permanent-magnet synchronous motor based on third-harmonic current reference online identification," *IEEE Access*, vol. 11, pp. 41840–41847, 2023, doi: 10.1109/ACCESS.2023.3269282.

[7] J. Rodriguez and P. Cortes, *Predictive Control of Power Converters and Electrical Drives*. Hoboken, NJ, USA: Wiley, 2012.

[8] M. Tang, C. Wang, and Y. Luo, "Predictive current control for permanent magnet synchronous motor based on internal model control observer," *Arch. Electr. Eng.*, vol. 71, no. 2, pp. 343–362, 2022, doi: 10.24425/aee.2022.140715.

[9] A. Yang and Z. Lu, "Multiscalar model-based predictive torque control without weighting factors and current sensors for induction motor drives," *IEEE J. Emerg. Sel. Topics Power Electron.*, vol. 10, no. 5, pp. 5785–5797, Oct. 2022, doi: 10.1109/JESTPE.2022.3181802.

[10] B. Tian, M. Molinas, and Q. An, "PWM investigation of a field-oriented controlled five-phase PMSM under two-phase open faults," *IEEE Trans. Energy Convers.*, vol. 36, no. 2, pp. 580–593, Jun. 2021, doi: 10.1109/TEC.2020.3029264.

[11] B. Tian, L. Sun, M. Molinas, and Q.-T. An, "Repetitive control based phase voltage modulation amendment for FOC-based five-phase PMSMs under single-phase open fault," *IEEE Trans. Ind. Electron.*, vol. 68, no. 3, pp. 1949–1960, Mar. 2021, doi: 10.1109/TIE.2020.2975502.

[12] W. Li, G. Feng, Z. Li, M. S. Toulabi, and N. C. Kar, "Extended Kalman filter based inductance estimation for dual three-phase permanent magnet synchronous motors under the single open-phase fault," *IEEE Trans. Energy Convers.*, vol. 37, no. 2, pp. 1134–1144, Jun. 2022, doi: 10.1109/TEC.2021.3129283.

[13] P. Song, W. Li, Z. Li, M. S. Toulabi, and N. C. Kar, "Noise and vibration prediction of a six-phase IPMSM in a single open-phase failure under a negative sequence current compensated fault tolerant control mode," *IEEE Trans. Magn.*, vol. 58, no. 8, pp. 1–6, Aug. 2022, doi: 10.1109/TMAG.2022.3146373.

[14] Z. Liu, Y. Li, and Z. Zheng, "A review of drive techniques for multiphase machines," *CES Trans. Electr. Mach. Syst.*, vol. 2, no. 2, pp. 243–251, Jun. 2018, doi: 10.30941/CESTEMS.2018.00030.

[15] L. Zhang, X. Zhu, R. Cui, and S. Han, "A generalized open-circuit fault-tolerant control strategy for FOC and DTC of five-phase fault-tolerant permanent-magnet motor," *IEEE Trans. Ind. Electron.*, vol. 69, no. 8, pp. 7825–7836, Aug. 2022, doi: 10.1109/TIE.2021.3106012.

[16] B. Chikondra, U. R. Muduli, and R. K. Behera, "Improved DTC technique for THL-NPC VSI fed five-phase induction motor drive based on VVs assessment over a wide speed range," *IEEE Trans. Power Electron.*, vol. 37, no. 2, pp. 1972–1981, Feb. 2022, doi: 10.1109/TPEL.2021.3102963.

[17] M. S. R. Saeed, W. Song, B. Yu, and X. Feng, "Generalized deadbeat solution for model predictive control of five-phase PMSM drives," *IEEE Trans. Power Electron.*, vol. 38, no. 4, pp. 5178–5191, Apr. 2023, doi: 10.1109/TPEL.2022.3228074.

[18] Y. Luo, K. Yang, and Y. Zheng, "Luenberger observer-based model predictive control for six-phase PMSM motor with localization error compensation," *IEEE Trans. Ind. Electron.*, vol. 70, no. 11, pp. 10800–10810, Nov. 2023, doi: 10.1109/TIE.2022.3229340.

[19] P. F. C. Gonçalves, S. M. A. Cruz, and A. M. S. Mendes, "Disturbance observer based predictive current control of six-phase permanent magnet synchronous machines for the mitigation of steady-state errors and current harmonics," *IEEE Trans. Ind. Electron.*, vol. 69, no. 1, pp. 130–140, Jan. 2022, doi: 10.1109/TIE.2021.3053885.

[20] G. Wang, G. Zhang, and D. Xu, *Position Sensorless Control Techniques for Permanent Magnet Synchronous Machine Drives*. Cham, Switzerland: Springer, 2020.

[21] R. Krishnan, *Permanent Magnet Synchronous and Brushless DC Motor Drives*. Boca Raton, FL, USA: CRC Press, 2010.

[22] A. Glumineau, J. De, and L. Morales, *Advances in Industrial Control Sensorless AC Electric Motor Control Robust Advanced Design Techniques and Applications*. Cham, Switzerland: Springer, 2015.

[23] J. Guzinski, H. Abu-Rub, and S. Patryk, *Variable Speed ac Drives with Inverter Output Filters*. Hoboken, NJ, USA: Wiley, 2015.

[24] F. Barrero and M. J. Duran, "Recent advances in the design, modeling, and control of multiphase machines—Part I," *IEEE Trans. Ind. Electron.*, vol. 63, no. 1, pp. 449–458, Jan. 2016, doi: 10.1109/TIE.2015.2447733.

[25] M. J. Duran and F. Barrero, "Recent advances in the design, modeling, and control of multiphase machines—Part II," *IEEE Trans. Ind. Electron.*, vol. 63, no. 1, pp. 459–468, Jan. 2016, doi: 10.1109/TIE.2015.2448211.

DEEPAK VYAS received the B.Eng. and M.Tech. degrees in India. He is currently pursuing the Ph.D. degree with the Faculty of Electrical and Control Engineering, Gdansk University of Technology.

His research interest includes control of the motor drive, backstepping control, sensorless control, multi-scalar control, and nonlinear control of electrical machines.

MARCIN MORAWIEC (Senior Member, IEEE) received the Ph.D. and D.Sc. degrees from Gdansk University of Technology, Gdańsk, Poland, in 2007 and 2017, respectively.

Since 2017, he has been an Associate Professor with Gdansk University of Technology. His main scientific activities are concentrated on multi-scalar models, nonlinear control of any electrical machines, sensorless control, nonlinear control, backstepping control, adaptive observer backstepping, and sliding mode control.

GRZEGORZ KOSTRO received the Ph.D. degree in electrical engineering, in 2007. He has been with Gdansk University of Technology, since 2007, the scope of his specialization is modeling, design, and diagnostics of electrical machines. He conducts research on the development of circuit models of electric machines using the Lagrange energy method, he also deals with the issues of designing electrical machines, in particular asynchronous machines with several phases greater than three, and low-speed synchronous generators with permanent magnets. He is the author or co-author of three patents and 74 articles.

ANDRZEJ JĄDERKO received the M.Sc. degree in electrical engineering from Czestochowa University of Technology, Częstochowa, Poland, in 1987, and the Ph.D. degree from Gdansk University of Technology, Gdańsk, Poland, in 1997. He is currently with the Department of Electrical Engineering, Czestochowa University of Technology. His scientific activities are concentrated on the control of drive systems, control of wind turbines, safety of electrical drives, and modern electricity storage. He is the author of over 70 articles and two chapters in monographs.

JANUSZ BARAN was born in Częstochowa, Poland, in 1961. He received the M.Sc. degree in electrical engineering from Czestochowa University of Technology, in 1985, and the Ph.D. degree in electrical engineering from Lublin University, in 1990. Since 1986, he has been with the Institute of Electronics and Control Systems, Czestochowa University of Technology. He is the author or co-author of more than 50 scientific publications. His research interests include the digital control of nonlinear systems and digital signal processing.